

Detailed Abundance Analysis of the Brightest Star in Segue 2, the Least Massive Galaxy^{*}

Ian U. Roederer^{1†} and Evan N. Kirby^{2,3‡}

¹*Department of Astronomy, University of Michigan, 500 Church Street, Ann Arbor, MI 48109, USA*

²*Department of Physics and Astronomy, University of California, 4129 Frederick Reines Hall, Irvine, CA 92697, USA*

³*Center for Galaxy Evolution Fellow*

13 March 2014

ABSTRACT

We present the first high resolution spectroscopic observations of one red giant star in the ultra-faint dwarf galaxy Segue 2, which has the lowest total mass (including dark matter) estimated for any known galaxy. These observations were made using the MIKE spectrograph on the Magellan II Telescope at Las Campanas Observatory. We perform a standard abundance analysis of this star, SDSS J021933.13+200830.2, and present abundances of 21 species of 18 elements as well as upper limits for 25 additional species. We derive $[\text{Fe}/\text{H}] = -2.9$, in excellent agreement with previous estimates from medium resolution spectroscopy. Our main result is that this star bears the chemical signatures commonly found in field stars of similar metallicity. The heavy elements produced by neutron-capture reactions are present, but they are deficient at levels characteristic of stars in other ultra-faint dwarf galaxies and a few luminous dwarf galaxies. The otherwise normal abundance patterns suggest that the gas from which this star formed was enriched by metals from multiple Type II supernovae reflecting a relatively well-sampled IMF. This adds to the growing body of evidence indicating that Segue 2 may have been substantially more massive in the past.

Key words: galaxies: individual (Segue 2) – nuclear reactions, nucleosynthesis, abundances – stars: abundances – stars: individual (SDSS J021933.13+200830.2).

1 INTRODUCTION

In the last decade, we have witnessed the discovery of extremely low-luminosity dwarf galaxies, largely due to the advent of the Sloan Digital Sky Survey (SDSS). The innovative searches for these galaxies were pioneered by Willman et al. (2005), Belokurov et al. (2007), and others. One member of this class of ultra-faint dwarf galaxies, Segue 2, was initially identified by Belokurov et al. (2009) as a stellar overdensity on the sky in images obtained as part of the Sloan Extension for Galactic Understanding and Exploration (SEGUE) and by using matched filters in colour-magnitude space. Deeper imaging and followup spectroscopy confirmed this detection, identified the presence of a cold velocity structure with a non-zero velocity dispersion, and indicated a mean metallicity of approximately $1/100^{\text{th}}$ solar.

Kirby et al. (2013) used the DEIMOS spectrograph to obtain red and near-infrared spectra of 25 probable members of Segue 2. These medium resolution spectra allowed Kirby et al. to constrain the line-of-sight velocity dispersion of Segue 2 to be $< 2.6 \text{ km s}^{-1}$ at 95 per cent confidence. This corresponds to a mass $< 2.1 \times 10^5 M_{\odot}$ within the half-light radius assuming Segue 2 is in dynamical equilibrium. That study also derived abundances of iron (Fe) and the α elements magnesium (Mg), silicon (Si), calcium (Ca), and titanium (Ti) for the 10 brightest members of Segue 2 based on fits to a grid of synthetic spectra. Kirby et al. confirmed that stars in Segue 2 span a range in metallicity of more than 1.5 dex. The $[\alpha/\text{Fe}]$ ratios in Segue 2 generally decrease with increasing $[\text{Fe}/\text{H}]$, as seen in classical dwarf galaxies (e.g., Shetrone et al. 2003; Kirby et al. 2011a) but not all of the ultra-faint dwarf galaxies (Frebel et al. 2010; Vargas et al. 2013). Segue 2 is the least-massive galaxy currently known based on its inferred dynamical mass. Yet with a mean metallicity of $[\text{Fe}/\text{H}] = -2.2$ it does not obey the mass-metallicity relationship established by Kirby et al. (2011b) for classical and ultra-faint dwarf galaxies. Segue 2, along with Segue 1 and Willman 1, may reveal the exis-

^{*} This paper includes data gathered with the 6.5 meter Magellan Telescopes located at Las Campanas Observatory, Chile.

[†] E-mail: iur@umich.edu

[‡] E-mail: ekirby@uci.edu

Table 1. Log of Observations

Date	UT mid-exposure	Exp. time (s)	Heliocentric V_r (km s ⁻¹)
2013 Dec 19	01:46	6600	-39.5
2013 Dec 20	01:47	6600	-39.6
2013 Dec 21	01:45	6600	-40.0
2013 Dec 22	01:49	4400	-39.9
2013 Dec 23	01:57	8000	-38.9

tence of a metallicity floor in galaxy formation. Alternatively, Segue 2 may have been substantially more massive before being tidally stripped down by a factor of several hundred in stellar mass to the remnant observed today.

We present the first high resolution spectroscopic observations of one red giant in Segue 2, SDSS J021933.13+200830.2, the only star reasonably bright enough for such observations. By coincidence, this star happens to be the most metal-poor star identified by Kirby et al. (2013) as a probable member. We use these data to confirm the radial velocity measured by Kirby et al. and derive detailed abundances of 21 species of 18 elements. We also present upper limits derived from non-detections of 25 additional species.

Throughout this work we adopt the standard definitions of elemental abundances and ratios. For element X, the logarithmic abundance is defined as the number of atoms of X per 10^{12} hydrogen atoms, $\log \epsilon(X) \equiv \log_{10}(N_X/N_H) + 12.0$. For elements X and Y, $[X/Y]$ is the logarithmic abundance ratio relative to the solar ratio, defined as $\log_{10}(N_X/N_Y) - \log_{10}(N_X/N_Y)_\odot$, using like ionization states; i.e., neutrals with neutrals and ions with ions. We adopt the solar abundances listed in Asplund et al. (2009). Abundances or ratios denoted with the ionization state indicate the total elemental abundance as derived from transitions of that particular state.

2 OBSERVATIONS

Only one star in Segue 2, SDSS J021933.13+200830.2, is bright enough for high-resolution spectroscopic observations. Its g magnitude, 17.18 ($V \approx 16.60$), is nevertheless quite faint when compared with the majority of metal-poor field red giants in the solar neighborhood that have comprised several large abundance surveys in recent decades. Spectroscopic observations of similar quality for other members of Segue 2 are not likely in the near future because the next-brightest probable member of Segue 2 is more than two magnitudes fainter.

Table 1 presents a record of our observations of SDSS J021933.13+200830.2. Observations were made with the Magellan Inamori Kyocera Echelle (MIKE) spectrograph (Bernstein et al. 2003) on the 6.5 m Landon Clay Telescope (Magellan II) at Las Campanas Observatory. These spectra were taken with the $0''.7 \times 5''.0$ slit, yielding a resolving power of $R \equiv \lambda/\Delta\lambda \sim 41,000$ in the blue and $R \sim 35,000$ in the red as measured from isolated ThAr lines in the comparison lamp images. This corresponds to ≈ 2.5 and 2.1 pixels per resolution element on the blue and red arms, respectively. The blue and red arms are split by a

dichroic at $\approx 4950 \text{ \AA}$. This setup achieves complete wavelength coverage from 3350–9150 \AA , although only the spectra longward of $\approx 4000 \text{ \AA}$ have signal sufficient to perform a detailed abundance analysis. Data reduction, extraction, sky subtraction, and wavelength calibration were performed using the MIKE data reduction pipeline written by D. Kelson (see Kelson 2003). Coaddition and continuum normalization were performed within IRAF.

Fig. 1 illustrates four sample regions of our spectrum of SDSS J021933.13+200830.2. Several prominent absorption features are indicated. After coaddition of the individual observations, totaling 8.9 h of integration, our spectrum of SDSS J021933.13+200830.2 has signal to noise (S/N) levels of 20, 55, 60, and 145 per pixel in the continuum at 3950, 4550, 5200, and 6750 \AA , respectively. SDSS J021933.13+200830.2 is a northern hemisphere target, and the differential refraction caused by observing at zenith angles $> 50^\circ$ is apparent in the compromised signal at blue wavelengths.

3 RADIAL VELOCITY MEASUREMENTS

We measure radial velocities (V_r) for each observation using the IRAF *fxcor* task to cross-correlate several individual orders with prominent absorption lines. The statistical uncertainties are smaller than 0.7 km s^{-1} per observation. We establish the velocity zeropoint by cross-correlating our highest S/N observation against a metal-poor velocity standard star, HD 128279, acquired previously and analyzed by Roederer et al. (2014a). We also obtained four high-S/N observations of the velocity standard star HD 83212, for which we measure $V_r = +109.3 \pm 0.2 \text{ km s}^{-1}$. This agrees well with the mean velocity published by Carney et al. (2003), $V_r = +109.13 \pm 0.16$, indicating that our velocity zeropoint is reliable at the $\approx 0.2 \text{ km s}^{-1}$ level. We measure a mean Heliocentric radial velocity for SDSS J021933.13+200830.2 of $V_r = -39.6 \pm 0.2 \text{ km s}^{-1}$. This is in excellent agreement with the value measured by Kirby et al. (2013) from moderate resolution DEIMOS spectra, $-41.0 \pm 2.0 \text{ km s}^{-1}$.

4 MODEL ATMOSPHERE PARAMETERS

We use one-dimensional model atmospheres interpolated from the ATLAS9 grid (Castelli & Kurucz 2003). We perform the analysis using a recent version of the spectral line analysis code MOOG (Snedden 1973; see discussion in Sobeck et al. 2011). Both ATLAS9 and MOOG assume that local thermodynamic equilibrium (LTE) holds in the line-forming layers.

We make several estimates of the effective temperature (T_{eff}) of SDSS J021933.13+200830.2. Ivezić et al. (2008) presented a colour- T_{eff} relationship tailored for SDSS broadband photometry; using the dereddened $g-r$ colour, their equation 3 predicts 4588 K. The set of Padova 12.6 Gyr isochrones (Girardi et al. 2002; Bressan et al. 2012) predicts 4597 K from the dereddened $g-i$ colour. Kirby et al. (2013) derived 4566 K from the DEIMOS spectrum based on a combination of photometry and spectroscopy. Following the techniques described by Kirby, Guhathakurta, & Sneden (2008) and Kirby et al. (2009, 2010), a χ^2 minimization algorithm determines which synthetic spectrum best

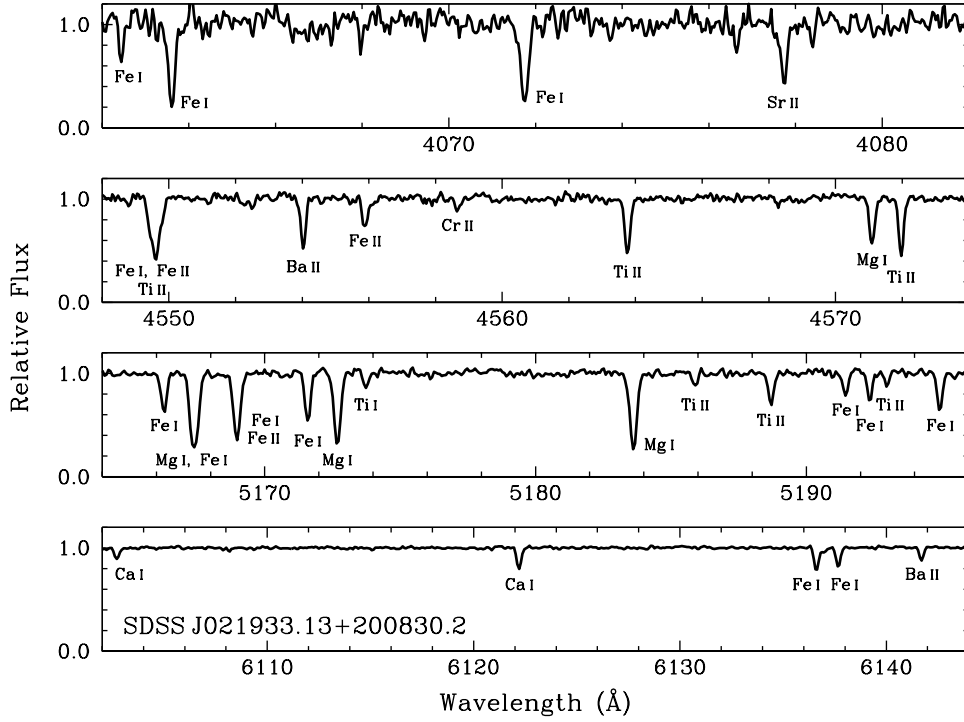


Figure 1. Four regions of the spectrum of SDSS J021933.13+200830.2, including several lines of interest. The species responsible for each absorption line is indicated.

matches the observed one. The temperature is allowed to vary but is constrained to a range of about 200 K around the photometrically-determined T_{eff} . These three estimates of T_{eff} agree well. Deriving T_{eff} by a more traditional spectroscopic approach, requiring that the iron abundances derived from Fe I lines show no trend with excitation potential, would demand a T_{eff} lower by nearly 350 K. In Fig. 2, we illustrate the region surrounding the H α line in SDSS J021933.13+200830.2 and HD 122563, a metal-poor giant with $T_{\text{eff}} = 4598 \pm 41$ K (Creevey et al. 2012). The line profiles are indistinguishable, suggesting the warmer temperatures are appropriate for SDSS J021933.13+200830.2. For consistency with Kirby et al. (2013), we adopt $T_{\text{eff}} = 4566$ K.

We calculate a physical surface gravity, $\log g$, based on standard stellar relations and the distance to Segue 2 estimated by the apparent magnitude of four blue horizontal branch stars (Belokurov et al. 2009). Other distance estimates by Ripepi et al. (2012)—who compared the Segue 2 fiducial sequence with that of globular cluster M68, and Boettcher et al. (2013)—who characterized the pulsation cycle of an RR Lyrae star in Segue 2, are consistent with the Belokurov et al. value. For a distance modulus of $m - M = 17.7 \pm 0.1$, our adopted $T_{\text{eff}} = 4566$ K, $T_{\text{eff}\odot} = 5777$ K, $\log g_{\odot} = 4.44$, $M_{\text{bol}\odot} = 4.74$, $g_0 = 16.46$, a bolometric correction, $BC_g = -1.05$ (Girardi et al. 2004), and a mass of $0.72 M_{\odot}$ (from the 12.6 Gyr isochrones of Bressan et al. 2012), we calculate $\log g = 1.36$. Reasonable uncertainties on these quantities imply an uncertainty in $\log g$ of no more than 0.10–0.15 dex.

We derive the microturbulence velocity, v_t , by requiring that the abundances derived from Fe I lines show no correlation with the reduced equivalent width, $\log(\text{EW}/\lambda)$. Our

derived value, 1.85 km s^{-1} , is in excellent agreement with the value calculated by Kirby et al. (2013), 1.87 km s^{-1} , using a relationship between $\log g$ and v_t .

We set the overall model metallicity, $[\text{M}/\text{H}]$, equal to the iron abundance derived from Fe II lines. We iteratively cull iron lines deviating by more than 2σ from the mean. The adopted model metallicity, $[\text{Fe II}/\text{H}] = -2.81$, is slightly higher than that derived from Fe I lines, $[\text{Fe I}/\text{H}] = -2.96$. We would need to lower $\log g$ by 0.45 dex to force these values to be equivalent, which seems unlikely based on the discussion above. This difference is what might be expected if the non-LTE effect of iron overionization is occurring (e.g., Thévenin & Idiart 1999). This difference is within the range found for cool metal-poor giants by Roederer et al. (2014a). If we were to adopt the cooler T_{eff} suggested by the iron excitation equilibrium method without adjusting $\log g$ accordingly, the difference between the iron abundances derived from Fe I and II would be nearly 0.8 dex. In order to compensate, we would have lowered v_t by 0.4 km s^{-1} , which is in the opposite sense than would be expected if SDSS J021933.13+200830.2 is a more evolved giant. We conclude by noting that our derived metallicity is in good agreement with what Kirby et al. (2013) found by fitting numerous iron lines in the red part of the spectrum, $[\text{Fe}/\text{H}] = -2.85 \pm 0.11$.

Roederer et al. (2014a) compared their derived model atmosphere parameters with those derived by a variety of different methods for stars in common. For red giants, the residuals had standard deviations of 151 K in T_{eff} , 0.40 in $\log g$, 0.41 km s^{-1} in v_t , and 0.24 dex in $[\text{Fe II}/\text{H}]$. For $\log g$ we retain the ≈ 0.15 dex uncertainty estimated previously, but for T_{eff} , v_t , and $[\text{M}/\text{H}]$ we adopt these values as the systematic uncertainty in the model atmosphere parameters.

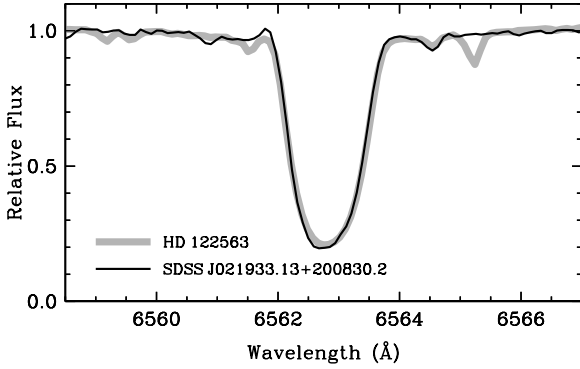


Figure 2. Profile of the H α line in SDSS J021933.13+200830.2 and HD 122563. The spectrum of HD 122563 was obtained using the same MIKE setup and presented by Roederer et al. (2014a).

5 ABUNDANCE ANALYSIS

Table 2 lists the line wavelength, species identification, excitation potential (E.P.) of the lower electronic energy level, and $\log gf$ value for each transition examined. Equivalent widths (EW), also listed in Table 2, are measured using a semi-automatic routine that fits Voigt absorption line profiles to continuum-normalized spectra (Roederer et al. 2014a). When a line is not detected, we derive 3σ upper limits on the abundance using a version of the formula presented on p. 590 of Frebel et al. (2008), which itself is derived from equation A8 of Bohlin et al. (1983). When multiple lines of the same species are not detected, we adopt the upper limit that provides the strongest constraint on the abundance.

Our abundance analysis closely follows that of Roederer et al. (2014a). Spectrum synthesis matching is performed for lines broadened by hyperfine splitting (hfs) or in cases where a significant isotope shift (IS) may be present. Linelists are generated using the Kurucz & Bell (1995) lists and updated using more recent experimental data when available. For unblended lines we use MOOG to compute theoretical EWs, which are then forced to match measured EWs by adjusting the abundance. For heavy elements with multiple isotopes, we adopt the r -process isotopic ratios presented in Sneden, Cowan, & Gallino (2008). We examine the stellar spectrum simultaneously with a spectrum of earth’s atmosphere (Hinkle et al. 2000) for all lines with $\lambda > 5670$ Å. We do not attempt to derive abundances from any of these lines when the telluric spectrum suggests they may be compromised. Carbon abundances, derived from the CH G band near 4300 Å, and nitrogen upper limits, derived from the violet and red CN bands near 3880 and 8000 Å are also found via spectrum synthesis matching.

Table 2 lists the abundances derived from each of the 260 features examined. We adopt corrections to account for departures from LTE for Na I lines (Lind et al. 2011) and K I lines (Takeda et al. 2002). These corrections amount to -0.35 , -0.33 , and -0.31 dex, respectively, for the Na I 5889, 5895, and K I 7698 Å lines. We also adopt the line-by-line corrections derived by Roederer et al. (2014a) to account for which lines are used in the analysis; these corrections are listed in Table 16 of that study.

Table 3 lists the mean abundances derived for SDSS J021933.13+200830.2. Weighted mean abundances and uncertainties are computed using the formalism pre-

sented in McWilliam et al. (1995), as discussed in detail in Roederer et al. We remind readers that the $[X/Fe]$ ratios are constructed by referencing abundances of element X, derived from neutral (ionized) species, to the iron abundance derived from Fe I (Fe II) lines. Several sets of uncertainties are listed in Table 3. The statistical uncertainty, $\sigma_{\text{statistical}}$, accounts for uncertainties in the EWs, $\log gf$ values, non-LTE corrections, and line-by-line offset corrections. The total uncertainty, σ_{total} , accounts for the statistical uncertainty and uncertainties in the model atmosphere parameters. The other two uncertainties listed in Table 3 are approximations to the abundance ratio uncertainties given by equations A19 and A20 of McWilliam et al. The quantity σ_{neutrals} for element A should be added in quadrature with $\sigma_{\text{statistical}}$ for element B when computing the ratio $[A/B]$ when B is derived from neutral lines. Similarly, σ_{ions} for element A should be added in quadrature with $\sigma_{\text{statistical}}$ for element B when element B is derived from ionized lines.

We note that comparisons with the abundance ratios derived by Kirby et al. (2013) are not particularly meaningful since the lines used in the present analysis are generally not covered by the DEIMOS spectrum. In principle this should not matter, but in practice the small number of weak Mg I and Si I lines that probably contribute most to the Kirby et al. results are all high excitation lines that are quite sensitive to the adopted value of T_{eff} in the model atmosphere. Noise may also be an issue when only a few features are present, as is the case in low metallicity stars. These effects may contribute to the different $[Mg/Fe]$ ratios ($+0.76 \pm 0.25$ found by Kirby et al.; $+0.31 \pm 0.21$ found here). The silicon abundances derived in our study may be unreliable (see Section 6), so we do not make a comparison with the $[Si/Fe]$ ratio derived by Kirby et al. The other ratios presented in Table 4 of Kirby et al. are in satisfactory agreement with those derived in the present study: for $[Fe I/H]$, -2.85 ± 0.11 and -2.96 ± 0.19 , respectively; for $[Ca/Fe]$, $+0.30 \pm 0.13$ and $+0.17 \pm 0.21$; and for $[Ti/Fe]$, -0.18 ± 0.31 and $+0.01 \pm 0.18$.

6 RESULTS

Figures 3 through 7 illustrate our derived abundance ratios for SDSS J021933.13+200830.2. Several other sets of abundances derived from high resolution spectroscopy are shown for comparison. Kirby et al. (2013) noted the similarity between the mean metallicity and abundance trends in Segue 2 and the more luminous classical dwarf spheroidal galaxy Ursa Minor, which they propose as a present-day analog of what Segue 2 once may have been in the tidal stripping scenario. We illustrate abundances in Ursa Minor using blue star symbols in Figures 3 through 7. These data are compiled from the high resolution observations of Shetrone, Côté, & Sargent (2001), Sadakane et al. (2004), Cohen & Huang (2010), and Kirby & Cohen (2012). Abundances in several ultra-faint dwarf galaxies (Boötes I, Coma Berenices, Hercules, Leo IV, Segue 1, Ursa Major II) are marked by the red diamonds. These data are compiled from Koch et al. (2008, 2013), Feltzing et al. (2009), Frebel et al. (2010), Norris et al. (2010a,b), Simon et al. (2010), Gilmore et al. (2013), and Ishigaki et al. (2014). We only illustrate each star once if it has been analyzed by mul-

Table 2. Atomic Data, Equivalent Widths, and Derived Abundances

Species	λ (Å)	E.P. (eV)	$\log gf$	Ref.	EW ^a (mÅ)	$\log \epsilon$	σ
Li I	6707.80	0.00	+0.17	1	...	< 0.28	...
C (CH)	$A^2\Delta - X^2\Pi$ G band			2	...	4.85	0.20
N (CN)	$B^2\Sigma - X^2\Sigma$ violet band			3	...	< 6.85	...
N (CN)	$A^2\Sigma - X^2\Sigma$ red band			3	...	< 9.00	...
[O I]	6300.30	0.00	-9.78	4	...	< 6.74	...
O I	7771.94	9.15	+0.37	4	...	< 6.68	...
O I	7774.17	9.15	+0.22	4	...	< 6.82	...
O I	7775.39	9.15	+0.00	4	...	< 7.16	...
Na I	5889.95	0.00	+0.11	4	189.2	3.45	0.49
Na I	5895.92	0.00	-0.19	4	161.1	3.42	0.53

The complete version of Table 2 is available online. An abbreviated version is shown here to demonstrate its form and content. References: (1) Smith, Lambert, & Nissen 1998 for both $\log gf$ value and ^7Li hfs; (2) B. Plez 2007, private communication; (3) Kurucz & Bell 1995; (4) Fuhr & Wiese 2009; (5) Chang & Tang 1990; (6) Aldenius et al. 2007; (7) Aldenius, Lundberg, & Blackwell-Whitehead 2009; (8) Lawler & Dakin 1989, using hfs from Kurucz & Bell 1995; (9) Lawler et al. 2013; (10) Pickering, Thorne, & Perez 2001, with corrections given in Pickering, Thorne, & Perez 2002; (11) Wood et al. 2013; (12) Doerr et al. 1985, using hfs from Kurucz & Bell 1995; (13) Biémont et al. 1989; (14) Sobek, Lawler, & Sneden 2007; (15) Nilsson et al. 2006; (16) Den Hartog et al. 2011 for both $\log gf$ value and hfs; (17) O’Brian et al. 1991; (18) Nitz et al. 1999, using hfs from Kurucz & Bell 1995; (19) Fuhr & Wiese 2009, using hfs from Kurucz & Bell 1995; (20) Roederer & Lawler 2012; (21) Biémont et al. 2011; (22) Ljung et al. 2006; (23) Palmeri et al. 2005; (24) Fuhr & Wiese 2009, using hfs/IS from McWilliam 1998 when available; (25) Lawler, Bonvallet, & Sneden 2001, using hfs from Ivans et al. 2006; (26) Lawler et al. 2009; (27) Li et al. 2007, using hfs from Sneden et al. 2009; (28) Den Hartog et al. 2003, using hfs/IS from Roederer et al. 2008 when available; (29) Lawler et al. 2006, using hfs/IS from Roederer et al. 2008 when available; (30) Lawler et al. 2001a, using hfs/IS from Ivans et al. 2006; (31) Den Hartog et al. 2006; (32) Roederer et al. 2012; (33) Lawler et al. 2001b, using hfs from Lawler, Wyart, & Blaise 2001 when available; (34) Wickliffe, Lawler, & Nave 2000; (35) Lawler, Sneden, & Cowan 2004 for both $\log gf$ value and hfs; (36) Lawler et al. 2008; (37) Wickliffe & Lawler 1997; (38) Sneden et al. 2009 for both $\log gf$ value and hfs/IS; (39) Lawler et al. 2007; (40) Ivarsson et al. 2003, using hfs/IS from Cowan et al. 2005—see note on $\log gf$ values there; (41) Biémont et al. 2000, using hfs/IS from Roederer et al. 2012.

^a Entries with no EW listed indicate that no line is detected or spectrum synthesis matching is used to derive an abundance.

multiple investigators, and we give preference to the highest quality observations. Figures 3 through 7 also include abundances from a sample of 98 metal-poor field red giant stars analyzed by Roederer et al. (2014a).

As seen in Fig. 3, the subsolar [C/Fe] ratio in SDSS J021933.13+200830.2 is typical for red giants that have experienced first dredge-up, which mixes products of the CN-cycle to the surface. Similar [C/Fe] ratios are found in stars belonging to the ultra-faint dwarf galaxies and Ursa Minor. Unfortunately, our upper limit on the nitrogen abundance is uninteresting and only constrains [N/Fe] < +1.81. Our upper limit on the oxygen abundance is also uninteresting, [O/Fe] < +0.95. Lithium is not detected in SDSS J021933.13+200830.2, but the upper limit we derive is similar to the upper limits commonly found in field red giants.

Fig. 3 also illustrates the ratios of α elements to iron. The [Mg/Fe] ratio in SDSS J021933.13+200830.2 is within one standard deviation of the field giants and falls within the range of [Mg/Fe] ratios found in Ursa Minor and the ultra-faint dwarf galaxies. This result is unchanged if other comparison samples of field stars are considered instead (e.g., Cayrel et al. 2004; Honda et al. 2004; Lai et al. 2008; Yong et al. 2013; Cohen et al. 2013). The [Si/Fe] ratio in SDSS J021933.13+200830.2 is lower by ≈ 0.6 dex than the [Si/Fe] ratios in field giants at similar metallicity. This abundance is derived from only one strong line, Si I 3905 Å, and the abundances inferred from this line are known to

anti-correlate with T_{eff} (e.g., Preston et al. 2006). This effect is minimized somewhat by our use of only the red giants in the Roederer et al. (2014a) sample for comparison, but fig. 27 of that study demonstrates that there is still a slight trend with T_{eff} even with this restriction. We discard the [Si/Fe] ratio from further consideration. The [Ca/Fe] ratio in SDSS J021933.13+200830.2 is on the low end of the distribution found in field stars of similar metallicity, typically at the 1–2 σ level depending on which comparison sample is used. Given the uncertainty in the [Ca/Fe] ratio for SDSS J021933.13+200830.2, ± 0.11 dex, and the typical dispersions in the [Ca/Fe] ratio for the comparison samples (≈ 0.10 – 0.15 dex for the samples listed above) this discrepancy is probably not significant. The [Ca/Fe] ratio in SDSS J021933.13+200830.2 is within the range found for Ursa Minor and the ultra-faint dwarf galaxies.

[Ti I/Fe] and [Ti II/Fe] are different by 0.26 dex, with [Ti II/Fe] being higher in SDSS J021933.13+200830.2. Bergemann (2011) calculates that the non-LTE corrections for [Ti I/Fe] are $\approx +0.2$ – 0.3 dex greater than for [Ti II/Fe] in HD 122563, which has similar stellar parameters to SDSS J021933.13+200830.2, and these corrections would bring [Ti I/Fe] and [Ti II/Fe] into agreement. Roederer et al. (2014a) identified a trend of increasing [Ti II/Ti I] with increasing metallicity (see fig. 54 there), which could be attributed to non-LTE effects. At [Fe/H] = -2.9 , that study found [Ti II/Ti I] $\approx +0.1$, ranging from -0.1 to $+0.3$ dex, which includes our de-

Table 3. Mean Abundances in SDSS J021933.13+200830.2

Species	N_{lines}	$\log \epsilon$	$[\text{X}/\text{Fe}]^a$	$\sigma_{\text{statistical}}$	σ_{total}	σ_{neutrals}	σ_{ions}
Fe I	96	4.54	−2.96	0.03	0.19	0.00	0.00
Fe II	10	4.69	−2.81	0.05	0.08	0.00	0.00
Li I	1	< 0.28
C (CH)	1	4.85	−0.52
N (CN)	1	< 6.85	< 1.81
O I	4	< 6.68	< 0.95
Na I	2	3.44	0.16	0.10	0.40	0.29	0.37
Mg I	5	4.95	0.31	0.03	0.21	0.05	0.18
Al I	1	2.89	−0.60	0.07	0.35	0.23	0.31
Si I	1	4.70	0.15	0.15	0.34	0.21	0.30
K I	1	2.37	0.30	0.12	0.22	0.13	0.20
Ca I	12	3.54	0.17	0.10	0.21	0.11	0.19
Sc II	6	0.53	0.19	0.03	0.07	0.16	0.06
Ti I	13	2.00	0.01	0.02	0.18	0.05	0.16
Ti II	25	2.42	0.28	0.03	0.07	0.16	0.06
V I	1	0.85	−0.12	0.10	0.21	0.11	0.18
V II	2	< 1.10	< −0.02
Cr I	7	2.39	−0.28	0.02	0.18	0.05	0.16
Cr II	2	3.01	0.18	0.04	0.08	0.17	0.07
Mn I	3	1.96	−0.51	0.02	0.18	0.05	0.16
Co I	1	1.64	−0.39	0.10	0.27	0.15	0.24
Ni I	4	3.33	0.08	0.10	0.21	0.11	0.19
Cu I	1	< 0.88	< −0.35
Zn I	2	1.97	0.37	0.02	0.18	0.05	0.16
Rb I	1	< 1.24	< 1.68
Sr II	2	−1.29	−1.35	0.02	0.29	0.27	0.26
Y II	2	< −1.53	< −0.93
Zr II	3	< −0.74	< −0.51
Tc I	1	< −0.04
Ba II	5	−1.62	−1.00	0.04	0.08	0.16	0.06
La II	4	< −1.74	< −0.03
Ce II	5	< −1.30	< −0.07
Pr II	4	< −1.59	< 0.50
Nd II	4	< −1.32	< 0.07
Sm II	1	< −1.41	< 0.44
Eu II	4	< −2.59	< −0.30
Gd II	3	< −0.79	< 0.95
Tb II	2	< −1.34	< 1.17
Dy II	3	< −1.30	< 0.41
Ho II	3	< −1.61	< 0.72
Er II	3	< −0.78	< 1.11
Tm II	2	< −1.38	< 1.33
Yb II	1	< −0.76	< 1.13
Hf II	2	< −0.47	< 1.49
Ir I	1	< 0.08	< 1.66
Pb I	1	< 0.93	< 1.85

^a $[\text{Fe}/\text{H}]$ is indicated for Fe I and Fe II

rived value for SDSS J021933.13+200830.2. $[\text{Ti I}/\text{Fe}]$ is on the low side of the distribution for field giants with similar metallicities; $[\text{Ti II}/\text{Fe}]$, however, is well within the normal range for field giants. For the atmospheric conditions found in SDSS J021933.13+200830.2, ground and low-lying levels of Ti II constitute the main reservoir of titanium atoms, so these levels cannot be significantly out of equilibrium (Lawler et al. 2013). When comparing ratios of one α element to another, however, the titanium abundance derived from Ti I lines may be preferable since the other α element abundances are also derived from transi-

tions of the neutral species. Regardless of whether $[\text{Ti I}/\text{Fe}]$ or $[\text{Ti II}/\text{Fe}]$ more accurately represents the $[\text{Ti}/\text{Fe}]$ ratio in SDSS J021933.13+200830.2, both are within the range found in Ursa Minor and the ultra-faint dwarfs.

Fig. 4 illustrates the $[\text{Na}/\text{Fe}]$, $[\text{Al}/\text{Fe}]$, and $[\text{K}/\text{Fe}]$ ratios. These three abundance ratios in SDSS J021933.13+200830.2 all coincide with the bulk of the same ratios in the field giants, Ursa Minor, and for $[\text{Na}/\text{Fe}]$ and $[\text{Al}/\text{Fe}]$ in the ultra-faint dwarf galaxies. Potassium has not been detected previously in any star in an ultra-faint dwarf galaxy, and the $[\text{K}/\text{Fe}]$ ratio in this one

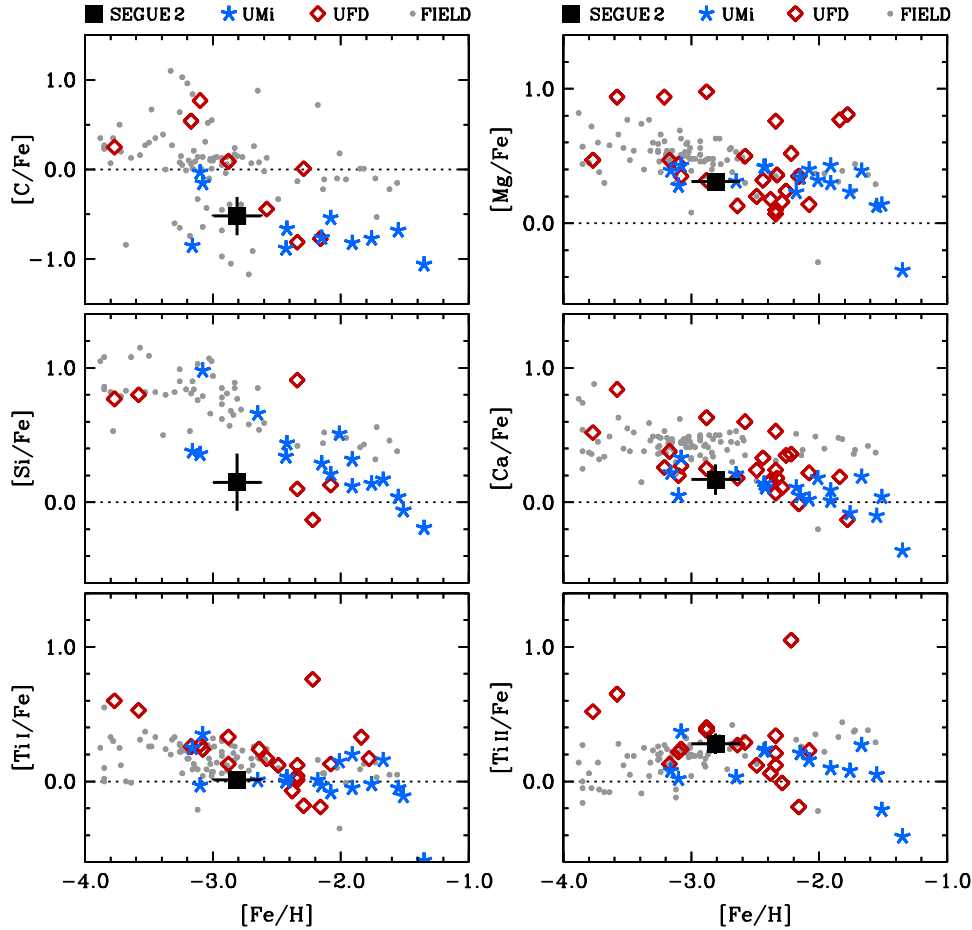


Figure 3. The $[C/Fe]$, $[Mg/Fe]$, $[Si/Fe]$, $[Ca/Fe]$, $[Ti\ I/Fe]$, and $[Ti\ II/Fe]$ ratios in SDSS J021933.13+200830.2 (“Segue 2”), the classical dwarf spheroidal galaxy Ursa Minor (“UMi”), several ultra-faint dwarf galaxies (“UFD”; Boötes I, Coma Berenices, Hercules, Leo IV, Segue 1, Ursa Major II) and a sample of field red giants. References for the comparison samples are listed in Section 6. The dotted lines represent the Solar ratios.

star in Segue 2 appears quite normal in comparison with the field giants and stars in Ursa Minor.

Fig. 5 illustrates the abundance ratios among the iron group elements in SDSS J021933.13+200830.2 and the comparison samples. In nearly all cases, the SDSS J021933.13+200830.2 ratios fall well within the ranges found in the comparison samples at similar metallicities. The $[Sc/Fe]$ ratio in SDSS J021933.13+200830.2 is ≈ 0.2 dex higher than the field giants, but it is within the range of the stars in ultra-faint dwarf galaxies. The $[Co/Fe]$ ratio in SDSS J021933.13+200830.2 is lower than the limited data available for stars in the ultra-faint dwarf galaxies, but it is within the range of field giants. These mild differences are probably not significant, and we conclude that the ratios among the iron group elements in SDSS J021933.13+200830.2 are normal for stars of this metallicity.

Fig. 6 illustrates the $[Sr/Fe]$ and $[Ba/Fe]$ ratios. Both ratios are deficient in SDSS J021933.13+200830.2 by more than an order of magnitude relative to the solar ratios. The $[Sr/Fe]$ ratio appears normal with respect to the ultra-faint dwarf galaxies, but it is noticeably lower than the $[Sr/Fe]$ ratios found in Ursa Minor or the field stars at similar metallicity. The $[Ba/Fe]$ ratio in SDSS J021933.13+200830.2 ap-

pears normal with respect to all of the comparison samples. The $[Sr/Ba]$ ratio in SDSS J021933.13+200830.2 is -0.35 ± 0.27 . For comparison, the five highly r -process enhanced field stars studied by Sneden et al. (2009) have a mean $[Sr/Ba]$ ratio of -0.16 ± 0.11 . Aoki et al. (2008) studied a sample of eight field stars with $[Fe/H] < -2$ and high levels of s -process enhancement. In contrast, the mean $[Sr/Ba]$ ratio in these stars was found to be -1.17 ± 0.18 . The $[Sr/Ba]$ ratio in SDSS J021933.13+200830.2 is in agreement with this ratio in the r -process enhanced stars but not with that in the s -process enhanced stars.

The $[Sr/Ba]$ ratio in SDSS J021933.13+200830.2 also falls within the normal range for other ultra-faint dwarf galaxies. This ratio varies by more than 2 dex within individual ultra-faint dwarf galaxies (Ursa Major II; Frebel et al. 2010) and among the ensemble of these systems. Four stars in Boötes I where Sr II and Ba II are detected indicate $[Sr/Ba]$ is significantly subsolar in that system, with $[Sr/Ba] = -0.9 \pm 0.3$ (Norris et al. 2010b; Ishigaki et al. 2014). Such low ratios are found among halo field stars, but they are rare; in the Roederer et al. (2014a) field star sample, only 11 per cent of the red giants have $[Sr/Ba] < -0.3$. The growing significance of this discrepancy between $[Sr/Ba]$

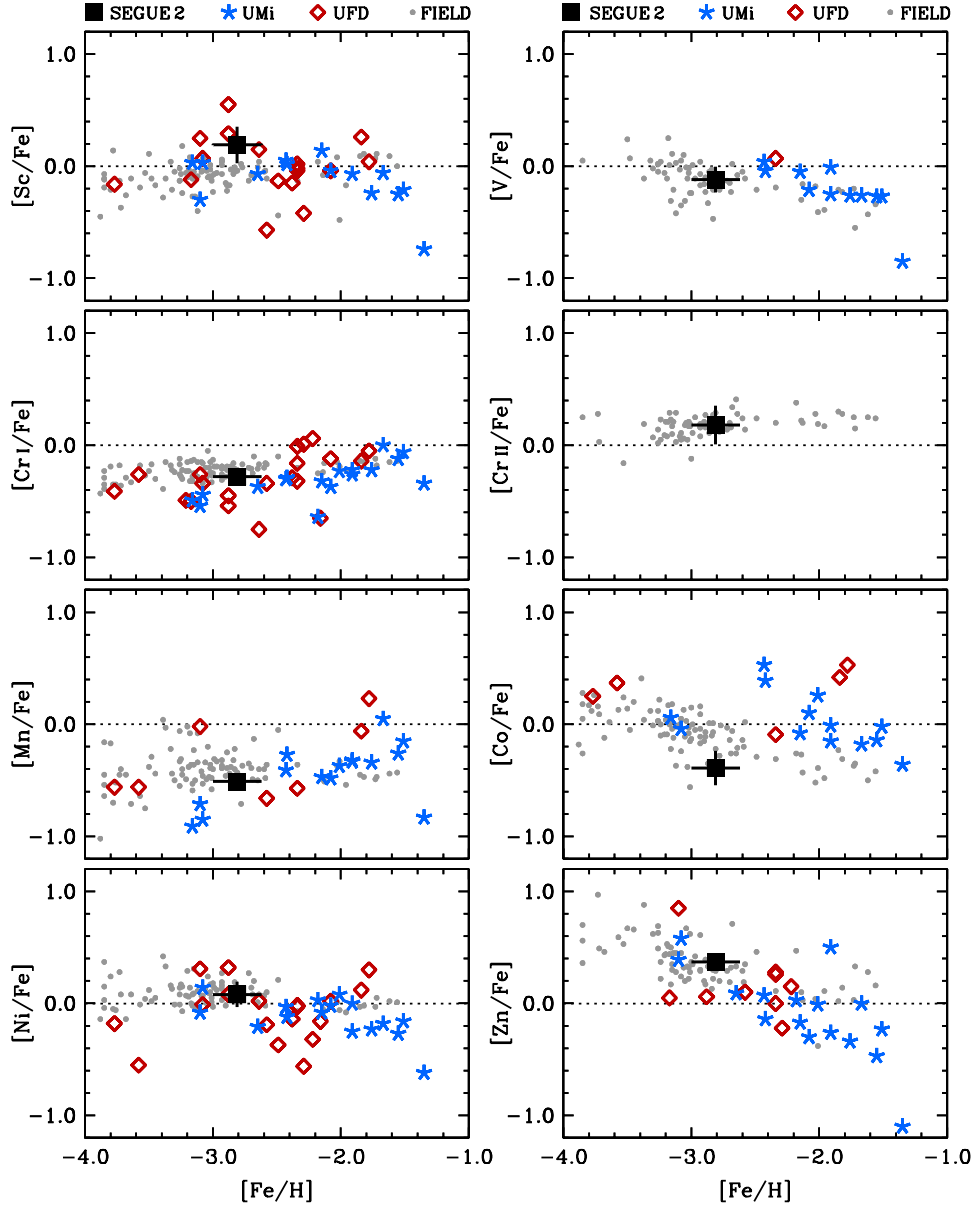


Figure 5. The $[\text{Sc}/\text{Fe}]$, $[\text{V}/\text{Fe}]$, $[\text{Cr I}/\text{Fe}]$, $[\text{Cr II}/\text{Fe}]$, $[\text{Mn}/\text{Fe}]$, $[\text{Co}/\text{Fe}]$, $[\text{Ni}/\text{Fe}]$, and $[\text{Zn}/\text{Fe}]$ ratios. Symbols are the same as in Fig. 3.

in field stars and the ultra-faint dwarf galaxies should be monitored as more data become available.

7 DISCUSSION

7.1 Metal Production in Segue 2

The $[\text{Mg}/\text{Fe}]$, $[\text{Ca}/\text{Fe}]$, and possibly $[\text{Ti}/\text{Fe}]$ ratios in SDSS J021933.13+200830.2 are enhanced relative to the solar ratios and are not subsolar like those found in the more metal-rich stars of classical Local Group dwarf galaxies. Neither the intermediate odd- Z elements (Na, Al, K) nor the iron group elements show any significant deviations from the abundance patterns commonly found in field stars or dwarf galaxies. Ratios among the neutron-capture elements and iron ($[\text{Sr}/\text{Fe}]$, $[\text{Ba}/\text{Fe}]$) are subsolar by more than 1 dex, but these deficiencies are common in the ultra-faint dwarf

galaxy populations and lie at the low ends of the halo star distributions. This abundance pattern can be attributed to enrichment by Type II supernovae.

In Type II supernovae, magnesium is produced via hydrostatic carbon and neon burning, and calcium is produced via oxygen burning during the explosion (e.g., Woosley & Weaver 1995). Fig. 7 illustrates that the $[\text{Mg}/\text{Ca}]$ ratio in SDSS J021933.13+200830.2 is the same as in the majority of stars in the field, Ursa Minor, and the ultra-faint dwarf galaxies with similar $[\text{Mg}/\text{H}]$ ratios. Fig. 3 of Feltzing et al. (2009) and Figures 20 and 21 of Venn et al. (2012) demonstrate that the $[\text{Mg}/\text{Ca}]$ ratios in several other classical and ultra-faint dwarf galaxies match this ratio within a factor of ≈ 2 , regardless of whether $[\text{Mg}/\text{Fe}]$ and $[\text{Ca}/\text{Fe}]$ are solar or supersolar.

To place this result in context, it may be helpful to examine stars with non-standard $[\text{Mg}/\text{Ca}]$ ratios. In the dwarf

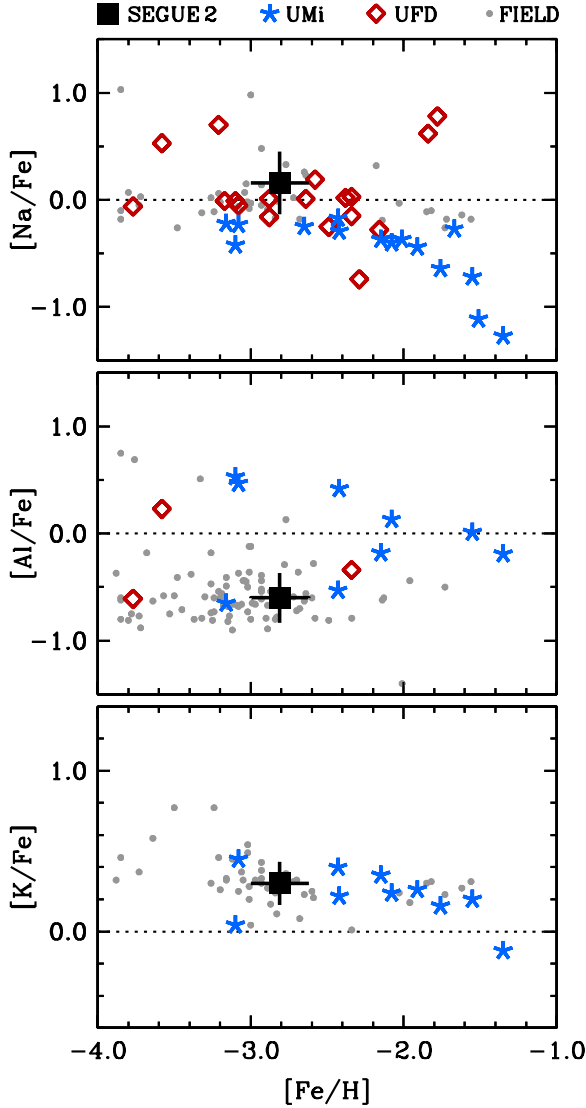


Figure 4. The $[\text{Na}/\text{Fe}]$, $[\text{Al}/\text{Fe}]$, and $[\text{K}/\text{Fe}]$ ratios. Symbols are the same as in Fig. 3.

galaxy population, these include one star found in Draco (Fulbright, Rich, & Castro 2004), two stars in Hercules (Koch et al. 2008), and one star in Carina (Venn et al. 2012). In these stars, the hydrostatic α elements O and Mg are enhanced relative to the explosive α element Ca. These authors interpreted the enhanced $[\text{Mg}/\text{Ca}]$ ratios as a consequence of stochastic sampling of the high end of the Type II supernova mass function. Gilmore et al. (2013) report a star in Boötes I, Boo-119, with a high $[\text{Mg}/\text{Ca}]$ ratio. This star also shows enhanced $[\text{C}/\text{Fe}]$ (Lai et al. 2011) and $[\text{Na}/\text{Fe}]$, suggesting it is a member of the class of carbon-enhanced metal-poor stars with no enhancement of neutron-capture elements. Such stars have been suggested as some of the earliest to have formed from the remnants of zero-metallicity Pop III stars (e.g., Norris et al. 2013). Feltzing et al. (2009) reported another star with enhanced $[\text{Mg}/\text{Ca}]$ in Boötes I, Boo-127, but that result was not confirmed by Gilmore et al. and Ishigaki et al. (2014). The similarity of the $[\text{Mg}/\text{Ca}]$ ratios in SDSS J021933.13+200830.2, the field giants, and most classical dwarfs suggest that the Type II supernovae

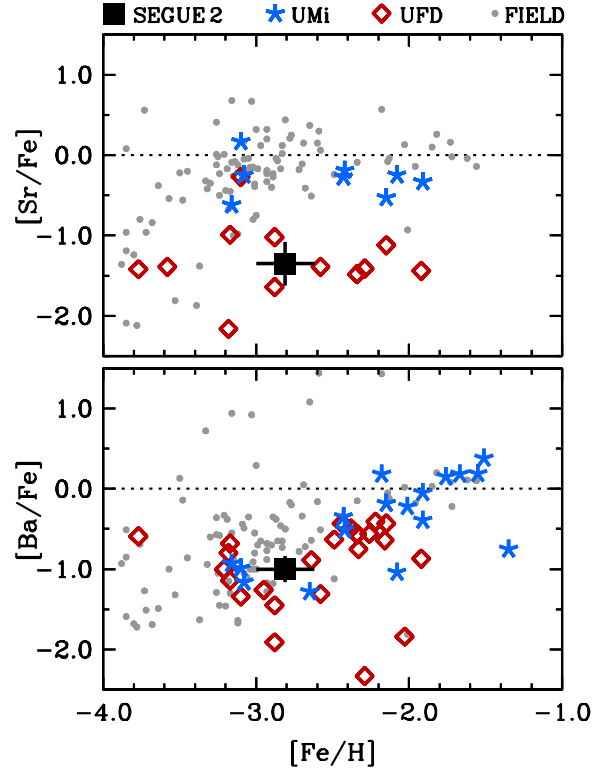


Figure 6. The $[\text{Sr}/\text{Fe}]$ and $[\text{Ba}/\text{Fe}]$ ratios. Symbols are the same as in Fig. 3.

reflect a relatively well-sampled initial mass function (IMF) in Segue 2.

Kirby et al. (2013) excluded inhomogeneous mixing as the source of the metallicity spread in Segue 2 on account of the dispersion in the $[\text{Si}/\text{Fe}]$ and $[\text{Ti}/\text{Fe}]$ ratios. Downward trends in these ratios (and possibly $[\text{Mg}/\text{Fe}]$) with increasing $[\text{Fe}/\text{H}]$ suggest that star formation in Segue 2 occurred over a timescale long enough to incorporate the products of multiple supernovae. Abundance information for more metal-rich stars in Segue 2 is limited to the $[\text{Mg}/\text{Fe}]$, $[\text{Si}/\text{Fe}]$, $[\text{Ca}/\text{Fe}]$, and $[\text{Ti}/\text{Fe}]$ ratios derived by Kirby et al. These data may indicate that the additional metals were manufactured by Type Ia supernovae, which produce intrinsically lower $[\alpha/\text{Fe}]$ ratios. McWilliam, Wallerstein, & Mottini (2013) offer an alternative hypothesis that better explains the declining $[\alpha/\text{Fe}]$ ratios and low ratios of hydrostatic to explosive α elements in the Sagittarius dwarf galaxy. In this scenario, an extension of that proposed initially by Tolstoy et al. (2003) for other classical dwarf galaxies, a low star formation rate produces a top-light IMF. The yields of hydrostatic α elements increase with increasing stellar mass, so they will naturally be deficient in such a scenario. The extant data are insufficient to distinguish between these scenarios in Segue 2, but the composition of at least one of the most metal-poor stars in Segue 2 is dominated by products of fairly normal Type II supernovae. Either way, the Kirby et al. abundance data indicate that Segue 2 experienced self-enrichment, excluding it from the list of candidates for the “one-shot enrichment” scenario proposed by Frebel & Bromm (2012).

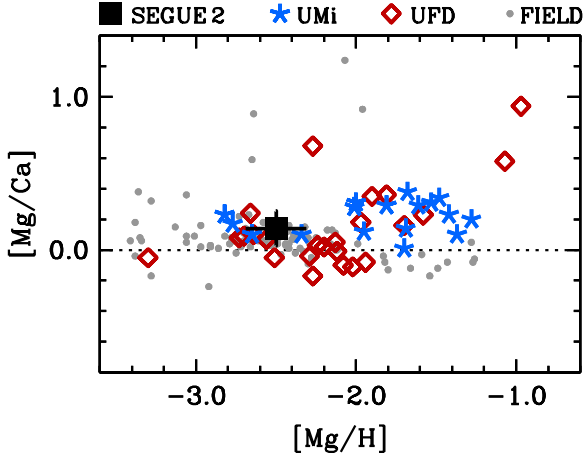


Figure 7. The $[\text{Mg}/\text{Ca}]$ ratios as a function of $[\text{Mg}/\text{H}]$. Symbols are the same as in Fig. 3.

7.2 The Original Mass of Segue 2

Segue 2 has a present-day stellar mass of $\approx 10^3 M_\odot$ (Kirby et al. 2013), assuming $M_*/L_V = 1.2$, as is typical for dwarf spheroidal galaxies (Woo, Courteau, & Dekel 2008). The $[\text{Sr}/\text{Fe}]$ ratio in Segue 2 more closely matches that found in the ultra-faint dwarf galaxies than in Ursa Minor. This could be an indication that the original mass of Segue 2 was not quite as large as the original mass of Ursa Minor. Similarly low $[\text{Sr}/\text{Fe}]$ ratios are also found, however, in a few stars in the more luminous systems Draco (Fulbright et al. 2004), Hercules (Koch et al. 2008), and Carina (Venn et al. 2012). We consider the low $[\text{Sr}/\text{Fe}]$ ratio in SDSS J021933.13+200830.2 inconclusive regarding the original mass of Segue 2.

On one hand, the total mass of metals, $\sim 0.1 M_\odot$, in a galaxy as small as Segue 2 is consistent with the predicted yields of a single zero-metallicity supernova (cf. Leo IV; Simon et al. 2010). Substantial metal loss from dwarf galaxies seems unavoidable, however, so multiple supernovae may be necessary to account for the small fractions of metals retained, even in the lowest metallicity stars. Kirby, Martin, & Finlator (2011) estimate that this fraction could be 1 per cent or less for dwarf galaxies like Ursa Minor. For a Salpeter (1955) IMF, only ~ 2 stars with $M > 8 M_\odot$ would be expected for every $10^3 M_\odot$ of stars formed. Tumlinson’s (2006) chemical evolution model predicts that the average halo star with $[\text{Fe}/\text{H}] \sim -3$ and normal abundance ratios has ~ 10 enriching progenitors. This model might also be applicable to SDSS J021933.13+200830.2 because this star has abundance ratios like halo stars of similar metallicity. Therefore, SDSS J021933.13+200830.2 might also require at least ~ 10 enriching progenitors to explain its chemical abundances, or ~ 5 times as many as would be expected from a Salpeter IMF for a galaxy with Segue 2’s current stellar mass. Consequently, we infer that the stellar mass of Segue 2 was at least ~ 5 times greater when it first formed stars than it is today.

Following a different line of reasoning, Kirby et al. (2013) estimated that Segue 2 must have had $\gtrsim 150$ times its current stellar mass in order to retain the ejecta of one supernova. This missing mass could be dark matter or

other stars that are no longer part of Segue 2. Kirby et al. also note that Segue 2 does not lie on the (present-day) luminosity-metallicity relation, which predicts that a galaxy of Segue 2’s luminosity should have a mean metallicity of $[\text{Fe}/\text{H}] = -2.83 \pm 0.16$ (Kirby et al. 2011b), a factor of 4 lower than derived by Kirby et al. (2013). Therefore Segue 2 would have shed ≈ 99.7 per cent of its original stellar mass if it obeyed the luminosity-metallicity relation at the time it was born. Presumably this mass loss would have occurred as Segue 2 fell into the Milky Way halo. Low surface brightness tidal tails have not yet been detected around Segue 2, and unfortunately no proper motions are available to calculate the orbit of Segue 2 with respect to the Milky Way.

7.3 The Origin of the Neutron-Capture Elements in Segue 2

Despite our best efforts, no heavy elements except strontium and barium can be detected in our spectrum of SDSS J021933.13+200830.2. In Section 6 we presented some typical r -process and s -process ratios of $[\text{Sr}/\text{Ba}]$ for comparison, and the $[\text{Sr}/\text{Ba}]$ ratio in SDSS J021933.13+200830.2 is suggestive of an r -process origin. Yet the $[\text{Sr}/\text{Ba}]$ ratio alone is hardly sufficient to unambiguously determine what kind of nucleosynthesis reactions may have produced the heaviest elements found in SDSS J021933.13+200830.2. Strontium may be produced by a myriad of neutron-capture and charged-particle reactions, and the abundance patterns resulting from r - and s -process nucleosynthesis depend on the physical conditions at the time of nucleosynthesis. The barium abundance and our upper limit on the europium abundance in SDSS J021933.13+200830.2 ($[\text{Eu}/\text{Ba}] < +0.70$) cannot exclude the main component of the r -process as exemplified by the abundance pattern in the metal-poor halo star CS 22892–052 (e.g., Sneden et al. 2003; $[\text{Eu}/\text{Ba}] = +0.65$). Prodigious lead production also did not occur, and the low $[\text{Sr}/\text{Fe}]$ and $[\text{Ba}/\text{Fe}]$ ratios suggest that large amounts of s -process material were not present in the gas from which SDSS J021933.13+200830.2 formed. Without additional information it is best to avoid making any definitive statements regarding the origin of the neutron-capture elements.

The unmistakable presence of strontium and barium in the most metal-poor star known in Segue 2 indicates that at least one neutron-capture nucleosynthesis mechanism operated prior to the formation of this star. Roederer (2013) showed that this is a characteristic of all other systems that have been studied, and our observations demonstrate that Segue 2 is no exception. Tumlinson’s (2006) model also predicts that ~ 90 per cent of the supernova progenitors of the average halo star with $[\text{Fe}/\text{H}] \sim -3$ are zero-metallicity progenitors. While this prediction remains unverified, the presence of neutron-capture elements in Segue 2 and all other systems hints that neutron-capture reactions may have occurred in at least some zero-metallicity stars (cf. Roederer et al. 2014b).

8 SUMMARY

We have performed a detailed abundance analysis of the brightest red giant star in the Segue 2 galaxy using high quality optical spectroscopy obtained with the MIKE spectrograph. The fundamental new insight from our analysis is that the composition of this star is not substantially different from the majority of stars in other ultra-faint dwarf galaxies or the most metal-poor stars in the classical dwarf galaxies like Ursa Minor. This suggests that multiple Type II supernovae were responsible for producing the metals observed in SDSS J021933.13+200830.2. For a standard Salpeter (1955) IMF, this implies that the stellar mass in Segue 2 was at least ~ 5 times greater than at the present. Our results echo those of Frebel et al. (2010) and Simon et al. (2010) that the light element abundance patterns in many of the ultra-faint dwarf galaxies generally match those found in halo stars. The exceptions appear to be the neutron-capture elements, which are persistently deficient in the ultra-faint dwarf galaxies.

ACKNOWLEDGMENTS

I.U.R. thanks J. Sobeck and C. Sneden for their expert assistance with MOOG. We thank the referee for providing helpful suggestions on the manuscript. This research has made use of NASA's Astrophysics Data System Bibliographic Services, the arXiv preprint server operated by Cornell University, the SIMBAD and VizieR databases hosted by the Strasbourg Astronomical Data Center, and the Atomic Spectra Database (Kramida et al. 2013) hosted by the National Institute of Standards and Technology. IRAF is distributed by the National Optical Astronomy Observatories, which are operated by the Association of Universities for Research in Astronomy, Inc., under cooperative agreement with the National Science Foundation. E.N.K. acknowledges support from the Southern California Center for Galaxy Evolution, a multicampus research program funded by the University of California Office of Research, and partial support from NSF grant AST-1009973.

REFERENCES

- Aldenius, M., Tanner, J. D., Johansson, S., Lundberg, H., Ryan, S. G. 2007, *A&A*, 461, 767
- Aldenius, M., Lundberg, H., Blackwell-Whitehead, R. 2009, *A&A*, 502, 989
- Aoki, W., et al. 2008, *ApJ*, 678, 1351
- Asplund, M., Grevesse, N., Sauval, A. J., Scott, P. 2009, *ARA&A*, 47, 481
- Belokurov, V., et al. 2007, *ApJ*, 654, 897
- Belokurov, V., et al. 2009, *MNRAS*, 397, 1748
- Bergemann, M. 2011, *MNRAS*, 413, 2184
- Bernstein, R., Sheckman, S. A., Gunnels, S. M., Mochnecki, S., Athey, A. E. 2003, *Proc. SPIE*, 4841, 1694
- Biémont, É., Grevesse, N., Faires, L. M., Marsden, G., Lawler, J. E. 1989, *A&A*, 209, 391
- Biémont, É., Garnir, H. P., Palmeri, P., Li, Z. S., Svanberg, S. 2000, *MNRAS*, 312, 116
- Biémont, É., et al. 2011, *MNRAS*, 414, 3350
- Boettcher, E., et al. 2013, *AJ*, 146, 94
- Bohlin, R. C., Hill, J. K., Jenkins, E. B., Savage, B. D., Snow, T. P., Spitzer, L., York, D. G. 1983, *ApJS*, 51, 277
- Bressan, A., Marigo, P., Girardi, L., Salasnich, B., Dal Cero, C., Rubele, S., Nanni, A. 2012, *MNRAS*, 427, 127
- Carney, B. W., Latham, D. W., Stefanik, R. P., Laird, J. B., Morse, J. A. 2003, *AJ*, 125, 293
- Castelli, F., Kurucz, R. L. *Proc. IAU Symp. No 210, Modelling of Stellar Atmospheres*, N. Piskunov et al., eds. 2003, A20 (arXiv:0405087)
- Cayrel, R., et al. 2004, *A&A*, 416, 1117
- Chang, T. N., Tang, X. 1990, *J. Quant. Spectrosc. Rad. Trans.*, 43, 207
- Cohen, J. G., Huang, W. 2010, *ApJ*, 719, 931
- Cohen, J. G., Christlieb, N., Thompson, I. B., McWilliam, A., Sheckman, S., Reimers, D., Wisotzki, L., Kirby, E. 2013, *ApJ*, 778, 56
- Cowan, J. J., et al. 2005, *ApJ*, 627, 238
- Creevey, O. L., et al. 2012, *A&A*, 545, A17
- Den Hartog, E. A., Lawler, J. E., Sneden, C., Cowan, J. J. 2003, *ApJS*, 148, 543
- Den Hartog, E. A., Lawler, J. E., Sneden, C., Cowan, J. J. 2006, *ApJS*, 167, 292
- Den Hartog, E. A., Lawler, J. E., Sobeck, J. S., Sneden, C., Cowan, J. J. 2011, *ApJS*, 194, 35
- Doerr, A., Kock, M., Kwiatkowski, M., Werner, K. 1985, *J. Quant. Spectrosc. Rad. Trans.*, 33, 55
- Feltzing, S., Eriksson, K., Kleyna, J., Wilkinson, M. I. 2009, *A&A*, 508, L1
- Frebel, A., Bromm, V. 2012, *ApJ*, 759, 115
- Frebel, A., Collet, R., Eriksson, K., Christlieb, N., Aoki, W. 2008, *ApJ*, 684, 588
- Frebel, A., Simon, J. D., Geha, M., Willman, B. 2010, *ApJ*, 708, 560
- Fuhr, J. R., Wiese, W. L. 2009, *Atomic Transition Probabilities*, published in the CRC Handbook of Chemistry and Physics, 90th Edition, ed. Lide, D. R., CRC Press, Inc., Boca Raton, FL, 10-93
- Fulbright, J. P., Rich, R. M., Castro, S. 2004, *ApJ*, 612, 447
- Gilmore, G., Norris, J. E., Monaco, L., Yong, D., Wyse, R. F. G., Geisler, D. 2013, *ApJ*, 763, 61
- Girardi, L., Bertelli, G., Bressan, A., Chiosi, C., Groenewegen, M. A. T., Marigo, P., Salasnich, B., Weiss, A. 2002, *A&A*, 391, 195
- Girardi, L., Grebel, E. K., Odenkirchen, M., Chiosi, C. 2004, *A&A*, 422, 205
- Hinkle, K., Wallace, L., Valenti, J., Harmer, D. 2000, *Visible and Near Infrared Atlas of the Arcturus Spectrum 3727-9300 Å*, Astron. Soc. Pac., San Francisco
- Honda, S., Aoki, W., Kajino, T., Ando, H., Beers, T. C., Izumiura, H., Sadakane, K., Takada-Hidai, M. 2004, *ApJ*, 607, 474
- Ishigaki, M. N., Aoki, W., Arimoto, N., Okamoto, S. 2014, *A&A*, 562, A146
- Ivans, I. I., Simmerer, J., Sneden, C., Lawler, J. E., Cowan, J. J., Gallino, R., Bisterzo, S. 2006, *ApJ*, 645, 613
- Ivarsson, S., et al. 2003, *A&A*, 409, 1141
- Ivezić, Ž., et al. 2008, *ApJ*, 684, 287
- Kelson, D. D. 2003, *PASP*, 115, 688
- Kirby, E. N., Cohen, J. G. 2012, *AJ*, 144, 168
- Kirby, E. N., Guhathakurta, P., Sneden, C. 2008, *ApJ*, 682, 1217

- Kirby, E. N., Guhathakurta, P., Bolte, M., Sneden, C., Geha, M. C. 2009, *ApJ*, 705, 328
- Kirby, E. N., et al. 2010, *ApJS*, 191, 352
- Kirby, E. N., Cohen, J. G., Smith, G. H., Majewski, S. R., Sohn, S. T., Guhathakurta, P. 2011a, *ApJ*, 727, 79
- Kirby, E. N., Lanfranchi, G. A., Simon, J. D., Cohen, J. G., Guhathakurta, P. 2011b, *ApJ*, 727, 78
- Kirby, E. N., Martin, C. L., Finlator, K. 2011, *ApJL*, 742, L25
- Kirby, E. N., Boylan-Kolchin, M., Cohen, J. G., Geha, M., Bullock, J. S., Kaplinghat, M. 2013, *ApJ*, 770, 16
- Koch, A., McWilliam, A., Grebel, E. K., Zucker, D. B., Belokurov, V. 2008, *ApJL*, 688, L13
- Koch, A., Feltzing, S., Adén, D., Matteucci, F. 2013, *A&A*, 554, A5
- Kramida, A., et al. 2013, NIST Atomic Spectra Database (version 5.1), available online: <http://physics.nist.gov/asd>
- Kurucz, R. L., Bell, B. 1995, Kurucz CD-ROM, Cambridge, MA: Smithsonian Astrophysical Observatory
- Lai, D. K., Bolte, M., Johnson, J. A., Lucatello, S., Heger, A., Woosley, S. E. 2008, *ApJ*, 681, 1524
- Lai, D. K., Lee, Y. S., Bolte, M., Lucatello, S., Beers, T. C., Johnson, J. A., Sivarani, T., Rockosi, C. M. 2011, *ApJ*, 738, 51
- Lawler, J. E., Dakin, J. T. 1989, *J. Opt. Soc. Am. B Optical Physics*, 6, 1457
- Lawler, J. E., Bonvallet, G., Sneden, C. 2001, *ApJ*, 556, 452
- Lawler, J. E., Wickliffe, M. E., den Hartog, E. A., Sneden, C. 2001a, *ApJ*, 563, 1075
- Lawler, J. E., Wickliffe, M. E., Cowley, C. R., Sneden, C. 2001b, *ApJS*, 137, 341
- Lawler, J. E., Wyart, J.-F., Blaise, J. 2001, *ApJS*, 137, 351
- Lawler, J. E., Sneden, C., Cowan, J. J. 2004, *ApJ*, 604, 850
- Lawler, J. E., Den Hartog, E. A., Sneden, C., Cowan, J. J. 2006, *ApJS*, 162, 227
- Lawler, J. E., Den Hartog, E. A., Labby, Z. E., Sneden, C., Cowan, J. J., Ivans, I. I. 2007, *ApJS*, 169, 120
- Lawler, J. E., Sneden, C., Cowan, J. J., Ivans, I. I., Den Hartog, E. A. 2009, *ApJS*, 182, 51
- Lawler, J. E., Sneden, C., Cowan, J. J., Wyart, J.-F., Ivans, I. I., Sobeck, J. S., Stockett, M. H., Den Hartog, E. A. 2008, *ApJS*, 178, 71
- Lawler, J. E., Guzman, A., Wood, M. P., Sneden, C., Cowan, J. J. 2013, *ApJS*, 205, 11
- Li, R., Chatelain, R., Holt, R. A., Rehse, S. J., Rosner, S. D., Scholl, T. J. 2007, *Phys. Scr.*, 76, 577
- Lind, K., Asplund, M., Barklem, P. S., Belyaev, A. K. 2011, *A&A*, 528, A103
- Ljung, G., Nilsson, H., Asplund, M., Johansson, S. 2006, *A&A*, 456, 1181
- McWilliam, A. 1998, *AJ*, 115, 1640
- McWilliam, A., Preston, G. W., Sneden, C., Searle, L. 1995, *AJ*, 109, 2757
- McWilliam, A., Wallerstein, G., Mottini, M. 2013, *ApJ*, 778, 149
- Nilsson, H., Ljung, G., Lundberg, H., Nielsen, K. E. 2006, *A&A*, 445, 1165
- Nitz, D. E., Kunau, A. E., Wilson, K. L., Lentz, L. R. 1999, *ApJS*, 122, 557
- Norris, J. E., Gilmore, G., Wyse, R. F. G., Yong, D., Frebel, A. 2010a, *ApJL*, 722, L104
- Norris, J. E., Yong, D., Gilmore, G., Wyse, R. F. G. 2010b, *ApJ*, 711, 350
- Norris, J. E., et al. 2013, *ApJ*, 762, 28
- O'Brian, T. R., Wickliffe, M. E., Lawler, J. E., Whaling, W., Brault, J. W. 1991, *J. Opt. Soc. Am. B Optical Physics*, 8, 1185
- Palmeri, P., Fischer, C. F., Wyart, J.-F., Godefroid, M. R. 2005, *MNRAS*, 363, 452
- Pickering, J. C., Thorne, A. P., Perez, R. 2001, *ApJS*, 132, 403
- Pickering, J. C., Thorne, A. P., Perez, R. 2002, *ApJS*, 138, 247
- Preston, G. W., Sneden, C., Thompson, I. B., Sheckman, S. A., Burley, G. S. 2006, *AJ*, 132, 85
- Ripepi, V., et al. 2012, *Memorie della Societa Astronomica Italiana Supplementi*, 19, 152
- Roederer, I. U. 2013, *AJ*, 145, 26
- Roederer, I. U., Lawler, J. E. 2012, *ApJ*, 750, 76
- Roederer, I. U., et al. 2012, *ApJS*, 203, 27
- Roederer, I. U., Lawler, J. E., Sneden, C., Cowan, J. J., Sobeck, J. S., Pilachowski, C. A. 2008, *ApJ*, 675, 723
- Roederer, I. U., Preston, G. W., Thompson, I. B., Sheckman, S. A., Sneden, C., Burley, G. S., Kelson, D. D. 2014a, *AJ*, in press
- Roederer, I. U., Preston, G. W., Thompson, I. B., Sheckman, S. A., Sneden, C., 2014b, *ApJ*, in press (arXiv:1402.4144)
- Sadakane, K., Arimoto, N., Ikuta, C., Aoki, W., Jablonka, P., Tajitsu, A. 2004, *PASJ*, 56, 1041
- Salpeter, E. E. 1955, *ApJ*, 121, 161
- Shetrone, M. D., Côté, P., Sargent, W. L. W. 2001, *ApJ*, 548, 592
- Shetrone, M., Venn, K. A., Tolstoy, E., Primas, F., Hill, V., Kaufer, A. 2003, *AJ*, 125, 684
- Simon, J. D., Frebel, A., McWilliam, A., Kirby, E. N., Thompson, I. B. 2010, *ApJ*, 716, 446
- Smith, V. V., Lambert, D. L., Nissen, P. E. 1998, *ApJ*, 506, 405
- Sneden, C. A. 1973, Ph.D. Thesis, Univ. of Texas at Austin
- Sneden, C., et al. 2003, *ApJ*, 591, 936
- Sneden, C., Cowan, J. J., Gallino, R. 2008, *ARA&A*, 46, 241
- Sneden, C., Lawler, J. E., Cowan, J. J., Ivans, I. I., Den Hartog, E. A. 2009, *ApJS*, 182, 80
- Sobeck, J. S., Lawler, J. E., Sneden, C. 2007, *ApJ*, 667, 1267
- Sobeck, J. S., et al. 2011, *AJ*, 141, 175
- Takeda, Y., Zhao, G., Chen, Y.-Q., Qiu, H.-M., Takada-Hidai, M. 2002, *PASJ*, 54, 275
- Thévenin, F., Idiart, T. P. 1999, *ApJ*, 521, 753
- Tolstoy, E., Venn, K. A., Shetrone, M., Primas, F., Hill, V., Kaufer, A., Szeifert, T. 2003, *AJ*, 125, 707
- Tumlinson, J. 2006, *ApJ*, 641, 1
- Vargas, L. C., Geha, M., Kirby, E. N., Simon, J. D. 2013, *ApJ*, 767, 134
- Venn, K. A., et al. 2012, *ApJ*, 751, 102
- Wickliffe, M. E., Lawler, J. E. 1997, *J. Opt. Soc. Am. B Optical Physics*, 14, 737
- Wickliffe, M. E., Lawler, J. E., Nave, G. 2000, *J. Quant. Spectrosc. Rad. Trans.*, 66, 363
- Willman, B., et al. 2005, *ApJL*, 626, L85
- Woo, J., Courteau, S., Dekel, A. 2008, *MNRAS*, 390, 1453

- Wood, M. P., Lawler, J. E., Sneden, C., Cowan, J. J. 2013, ApJS, 208, 27
Woosley, S. E., Weaver, T. A. 1995, ApJS, 101, 181
Yong, D., et al. 2013, ApJ, 762, 26